# Stator and Rotor Flux Based Deadbeat Direct Torque Control of Induction Machines

Barbara H. Kenny
Glenn Research Center, Cleveland, Ohio

Robert D. Lorenz
University of Wisconsin, Madison, Madison, Wisconsin

The NASA STI Program Office . . . in Profile

Since its founding, NASA has been dedicated to the advancement of aeronautics and space science. The NASA Scientific and Technical Information (STI) Program Office plays a key part in helping NASA maintain this important role.

The NASA STI Program Office is operated by Langley Research Center, the Lead Center for NASA's scientific and technical information. The NASA STI Program Office provides access to the NASA STI Database, the largest collection of aeronautical and space science STI in the world. The Program Office is also NASA's institutional mechanism for disseminating the results of its research and development activities. These results are published by NASA in the NASA STI Report Series, which includes the following report types:
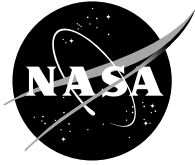
- TECHNICAL PUBLICATION. Reports of completed research or a major significant phase of research that present the results of NASA programs and include extensive data or theoretical analysis. Includes compilations of significant scientific and technical data and information deemed to be of continuing reference value. NASA's counterpart of peer-reviewed formal professional papers but has less stringent limitations on manuscript length and extent of graphic presentations.

- TECHNICAL MEMORANDUM. Scientific and technical findings that are preliminary or of specialized interest, e.g., quick release reports, working papers, and bibliographies that contain minimal annotation. Does not contain extensive analysis.

- CONTRACTOR REPORT. Scientific and technical findings by NASA-sponsored contractors and grantees.

- CONFERENCE PUBLICATION. Collected papers from scientific and technical conferences, symposia, seminars, or other meetings sponsored or cosponsored by NASA.

- SPECIAL PUBLICATION. Scientific, technical, or historical information from NASA programs, projects, and missions, often concerned with subjects having substantial public interest.

- TECHNICAL TRANSLATION. English-language translations of foreign scientific and technical material pertinent to NASA's mission.

Specialized services that complement the STI Program Office's diverse offerings include creating custom thesauri, building customized databases, organizing and publishing research results . . . even providing videos.

For more information about the NASA STI Program Office, see the following:

- Access the NASA STI Program Home Page at *http://www.sti.nasa.gov*

- E-mail your question via the Internet to help@sti.nasa.gov

- Fax your question to the NASA Access Help Desk at 301–621–0134

- Telephone the NASA Access Help Desk at 301–621–0390

- Write to:
  NASA Access Help Desk
  NASA Center for AeroSpace Information
  7121 Standard Drive
  Hanover, MD 21076

NASA/TM—2001-211100/REV1

# Stator and Rotor Flux Based Deadbeat Direct Torque Control of Induction Machines

Barbara H. Kenny
Glenn Research Center, Cleveland, Ohio

Robert D. Lorenz
University of Wisconsin, Madison, Madison, Wisconsin

September 2002

Available from

NASA Center for Aerospace Information
7121 Standard Drive
Hanover, MD 21076

National Technical Information Service
5285 Port Royal Road
Springfield, VA 22100

Available electronically at http://gltrs.grc.nasa.gov

## Document Change History

This printing, numbered as **NASA/TM—2001-211100/REV1, September 2002,** replaces the previous version in its entirety, **NASA/TM—2001-211100, September 2001**.

# Stator and Rotor Flux Based Deadbeat Direct Torque Control
## of Induction Machines

Barbara H. Kenny
National Aeronautics and Space Administration
Glenn Research Center
Cleveland, Ohio 44135

Robert D. Lorenz
University of Wisconsin, Madison
Madison, Wisconsin 53706

*Abstract*—**A new, deadbeat type of direct torque control is proposed, analyzed and experimentally verified in this paper. The control is based on stator and rotor flux as state variables. This choice of state variables allows a graphical representation which is transparent and insightful. The graphical solution shows the effects of realistic considerations such as voltage and current limits. A position and speed sensorless implementation of the control, based on the self-sensing signal injection technique, is also demonstrated experimentally for low speed operation. The paper first develops the new, deadbeat DTC methodology and graphical representation of the new algorithm. It then evaluates feasibility via simulation and experimentally demonstrates performance of the new method with a laboratory prototype including the sensorless methods.**

## I. INTRODUCTION

Direct torque control of induction machines has increasingly become an alternative to field orientation methods [1,2]. The classical method of direct torque control involves the use of a look-up table to select voltage vectors based on torque and stator flux magnitude error [3]. There is no current regulator, no pulse width modulation (PWM), nor reference frame transformations as in field orientation. With appropriately high sample rates this leads to fast torque response and low ripple. In addition, at operating conditions where the stator flux vector can be estimated accurately from the terminal voltage and current, this technique is also position and speed sensorless. However, at extremely low and zero speeds, the sensorless implementation of this technique suffers the same performance degradation as any control technique based on the estimate of stator flux using only fundamental voltage and current.

An alternative method of direct torque control is based on the deadbeat (inverse) solution to the machine equations [4–7]. The deadbeat solution is similar to the classical direct torque control method in that it controls torque and stator flux directly, without an intermediate current loop. It is different, however, in the calculation of the voltage vector to be applied to the machine. In the deadbeat solution, an inverse model is used to calculate the theoretical voltage vector needed to move the machine torque and stator flux to the desired values in one sample period. This voltage vector is then synthesized over the sample period by the use of PWM modulation techniques. However, the calculation of the voltage vector requires the solution of a quadratic equation with several parameter dependent coefficients. Insight into the operation of the control is lost with a purely algebraic approach to the solution of the quadratic equations.

This paper presents a new direct torque control strategy where stator and rotor flux are chosen as state variables in the deadbeat solution [8,9]. The use of stator and rotor flux as state variables, represented in the stator flux oriented synchronous reference frame, allows the construction of an intuitive graphical depiction of the necessary voltage vector to achieve the commanded torque and stator flux magnitude values in one time step. The graphical depiction changes as operating conditions or parameters vary; thus the resulting change in the necessary voltage vector can clearly be seen. Conversely, the impact of the selection of the wrong voltage vector on both the stator flux and torque errors can also be seen. In addition, practical operating limits can be shown on the same graph, thus presenting a good visualization of the current and voltage limitations. It is further shown that the structure of this control strategy is suitable for use with the self-sensing position estimation technique [10]. This enables low and zero speed position and speed sensorless direct torque control.

## II. FORMULATION OF A STATOR-ROTOR FLUX DEADBEAT CONTROL ALGORITHM

The state equations for the induction machine, using the stator and rotor flux as state variables in the stationary reference frame, are as follows [11].

$$p\boldsymbol{\lambda}_{qds} = \mathbf{V}_{qds} - \left(\frac{R_s}{\sigma L_s}\right)\boldsymbol{\lambda}_{qds} + \left(\frac{R_s L_m}{\sigma L_s L_r}\right)\boldsymbol{\lambda}_{qdr} \quad (1)$$

$$p\boldsymbol{\lambda}_{qdr} = \left(-\frac{R_r}{\sigma L_r} + j\omega_r\right)\boldsymbol{\lambda}_{qdr} + \left(\frac{L_m R_r}{L_r \sigma L_s}\right)\boldsymbol{\lambda}_{qds} \quad (2)$$

$$\tau_e = \frac{3P L_m}{4\sigma L_s L_r}\{\boldsymbol{\lambda}_{qds} \times \boldsymbol{\lambda}_{qdr}\} \quad (3)$$

A discrete time form of (1)–(3) is shown in (4)–(6) that is valid for small values of the sample time, $t_s$, for which the rotor speed, $\omega_r$, changes negligibly [8,9].

$$\boldsymbol{\lambda}_{qds}(k+1) - \boldsymbol{\lambda}_{qds}(k) =$$
$$\mathbf{V}_{qds}(k)t_s - \left(\frac{R_s}{\sigma L_s}\right)\boldsymbol{\lambda}_{qds}(k)t_s + \left(\frac{R_s L_m}{\sigma L_s L_r}\right)\boldsymbol{\lambda}_{qdr}(k)t_s \quad (4)$$

$$\boldsymbol{\lambda}_{qdr}(k+1) - \boldsymbol{\lambda}_{qdr}(k) =$$
$$\left(-\frac{R_r}{\sigma L_r} + j\omega_r\right)\boldsymbol{\lambda}_{qdr}(k)t_s + \left(\frac{L_m R_r}{L_r \sigma L_s}\right)\boldsymbol{\lambda}_{qds}(k)t_s \quad (5)$$

$$\tau_e(k+1) = \frac{3P L_m}{4\sigma L_s L_r}\{\boldsymbol{\lambda}_{qds}(k+1) \times \boldsymbol{\lambda}_{qdr}(k+1)\} \quad (6)$$

Equations (4)–(6) can be combined to form an expression for the change in torque, $\Delta\tau_e(k) = \tau_e(k+1) - \tau_e(k)$. If the d-axis of the excitation reference frame is aligned with the stator flux and the terms proportional to $t_s^2$ are neglected, a very useful relationship results as shown in (7) [8,9].

$$\frac{\Delta\tau_e(k)}{t_s} = \tau_e(k)\left(\frac{-R_r}{\sigma L_r} - \frac{R_s}{\sigma L_s}\right) + \frac{3PL_m}{4\sigma L_s L_r}$$
$$\left\{-\omega_r \lambda_{ds}^e(k) \lambda_{dr}^e(k) + V_{qs}^e(k) \lambda_{dr}^e(k) - V_{ds}^e(k) \lambda_{qr}^e(k)\right\} \quad (7)$$

Equation (7) can be rearranged as follows to show the linear relationship between $V_{qs}^e(k)t_s$ and $V_{ds}^e(k)t_s$ values which can be used to provide a given value of $\Delta\tau_e(k)$.

$$V_{qs}^e(k)\, t_s = \frac{4\sigma L_s L_r}{3PL_m \lambda_{dr}^e(k)}\left(\Delta\tau_e(k) + \tau_e(k)\left(\frac{R_r}{\sigma L_r} + \frac{R_s}{\sigma L_s}\right)t_s\right)$$
$$+ \omega_r \lambda_{ds}^e(k)\, t_s + V_{ds}^e(k)\, t_s \frac{\lambda_{qr}^e(k)}{\lambda_{dr}^e(k)} \quad (8)$$

If (8) is plotted in a d-q plane with $V_{ds}^e(k)t_s$ and $V_{qs}^e(k)t_s$ as the d- and q-axis variables respectively, the voltage loci for a given $\Delta\tau_e(k)$ is a straight line. This line is parallel to the rotor flux vector, $\lambda_{qdr}^e(k)$, as shown in Fig. 1 [8,9]. (Figs. 1–6 use the convention $f_{qd}=f_q-jf_d$.)
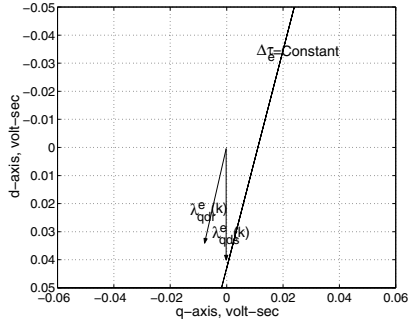


Fig. 1.  Constant $\Delta\tau_e(k)$ line

One representation of the multiple possible voltage (volt-sec) vectors $[V_{qs}^e(k)t_s \; V_{ds}^e(k)t_s]$ that could yield the desired change in motor torque, $\Delta\tau_e(k)$, is shown in Fig. 2.
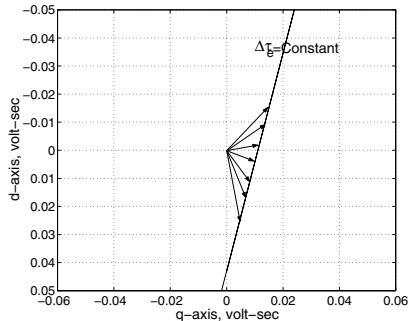


Fig. 2.  Graphical representation of multiple voltage vectors for machine torque change $\Delta\tau_e$

From (4) the discrete time expression for stator flux, neglecting stator resistance, is

$$\lambda_{qds}(k+1) - \lambda_{qds}(k) = V_{qds}(k)t_s. \quad (9)$$

Equation (9) can also be shown graphically. Figure 3 shows the plot of $|\lambda_{qds}(k+1)|$ and $\lambda_{ds}^e(k)$, where $\lambda_{ds}^e(k) = |\lambda_{qds}(k)|$. There are multiple voltage vectors, scaled by $t_s$, which will move the flux magnitude from a value of $\lambda_{ds}^e(k)$ to $|\lambda_{qds}(k+1)|$.
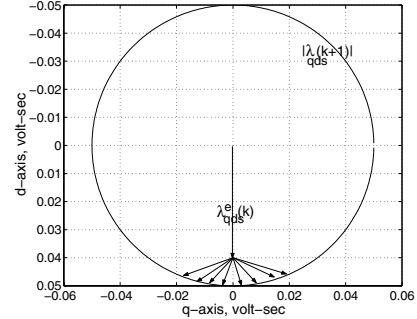


Fig. 3. Graphical representation of multiple voltage vectors for flux magnitude increase

The flux circle shown in Fig. 3 can be redrawn to show the change in flux magnitude, $\Delta|\lambda_{qds}(k)| = |\lambda_{qds}(k+1)| - \lambda_{ds}^e(k)$, where $\lambda_{ds}^e(k) = |\lambda_{qds}(k)|$. This circle is centered on the present value of stator flux, $\lambda_{ds}^e(k)$, with a radius equal to the magnitude $|\lambda_{qds}(k+1)|$. This adjustment means that the possible voltage (volt-sec) vector loci shown in Figs. 2 and 3 now all begin at the origin of the plot. Thus, for a given set of $\Delta\tau_e(k)$ and $\Delta|\lambda_{qds}(k)|$ requirements, the voltage vector which will solve both conditions simultaneously can be determined from the intersection of the $\Delta\tau_e(k)$ line and the $\Delta|\lambda_{qds}(k)|$ circle. This is shown in Fig. 4.
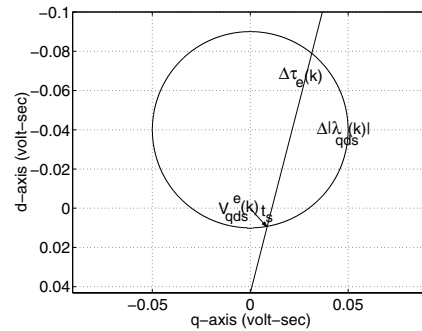


Fig. 4.  Graphical representation of a voltage vector which satisfies both $\Delta\tau_e(k)$ and $\Delta|\lambda_{qds}(k)|$ requirements

The equation defining the $\Delta|\lambda_{qds}(k)|$ circle is given in (10). The voltage vector which will solve both the $\Delta\tau_e(k)$ and the $\Delta|\lambda_{qds}(k)|$ requirements can be found mathematically from the simultaneous solution of (8) and (10), or graphically as shown in Fig. 4.

$$\left(V_{qs}^e(k)t_s\right)^2 + \left(V_{ds}^e(k)t_s - \lambda_{ds}^e(k)\right)^2 = |\lambda_{qds}(k+1)|^2 \quad (10)$$

The solution, $V_{qds}^e(k)t_s$, to the intersection of the $\Delta\tau_e(k)$ line and the $\Delta|\lambda_{qds}(k)|$ circle is bounded by the available dc bus voltage, the sample time and the inverter current limit. The range of voltages that can be synthesized from a two-level inverter can be represented as a hexagon in the d-q plane [11]. Thus the bound for $V_{qds}^e(k)t_s$ is a hexagon with

sides equal to $2/3\, V_{dc}\, t_s$ as shown in Fig. 5. The hexagon is shown at a static position in Fig. 5 but it actually rotates at the synchronous speed because the figure is in the synchronous reference frame.
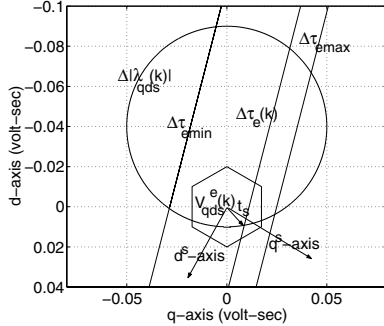


Fig. 5. Graphical representation of voltage and current limits on the possible voltage vector solutions

Figure 5 also shows the maximum and minimum values of $\Delta\tau_e$ based on a steady state solution using the inverter current limit, $|\mathbf{i}_{qdsmax}|$ and the present value of $\tau_e(k)$. The maximum torque can be calculated as a function of the stator flux magnitude and the maximum stator current as follows. For a stator flux oriented system, the torque can be expressed as

$$\tau_e = \frac{3P}{4}\,\lambda_{ds}\, i_{qs} \tag{11}$$

In terms of current magnitude, this becomes

$$\tau_e = \pm\frac{3P}{4}\,\lambda_{ds}\sqrt{|\mathbf{i}_{qds}|^2 - i_{ds}^2} \tag{12}$$

The variables $i_{ds}$ and $\lambda_{ds}$ can be related through the slip frequency by using the following two relationships which are given in [11].

$$\boldsymbol{\lambda}_{qds} = L_{\sigma s}\mathbf{i}_{qds} + \frac{L_m}{L_r}\boldsymbol{\lambda}_{qdr} \tag{13}$$

$$p\boldsymbol{\lambda}_{qdr} = \left(\frac{-R_r}{L_r} - j\omega_e + j\omega_r\right)(\boldsymbol{\lambda}_{qdr}) + \left(\frac{L_m R_r}{L_r}\right)\mathbf{i}_{qds} \tag{14}$$

Assuming stator flux orientation and steady state conditions, (13) and (14) can be used to form an expression for $i_{ds}$ in terms of the stator current magnitude and the stator flux.

$$i_{ds} = \frac{L_{\sigma s}L_s|\mathbf{i}_{qds}|^2 + \lambda_{ds}^2}{\lambda_{ds}L_s(1+\sigma)} \tag{15}$$

Equation (15) can be substituted into (12) to find a condition on the maximum torque that is possible for a specified maximum stator current magnitude and stator flux value.

$$\tau_{emax} = \pm\frac{3P}{4}\,\lambda_{ds}\sqrt{\mathbf{i}_{qdsmax}^2 - \left(\frac{L_{\sigma s}L_s|\mathbf{i}_{qdsmax}|^2 + \lambda_{ds}^2}{\lambda_{ds}L_s(1+\sigma)}\right)^2} \tag{16}$$

Finally, using (16) and the present value of torque, the maximum and minimum change in torque can be calculated.

$$\Delta\tau_{emax} = +\tau_{emax} - \tau_e(k) \tag{17}$$

$$\Delta\tau_{emin} = -\tau_{emax} - \tau_e(k) \tag{18}$$

It is interesting to consider the plot for a steady state condition ($\Delta\tau_e(k)=0$, $\Delta|\boldsymbol{\lambda}_{qds}(k)|=0$). This is shown in Fig. 6.
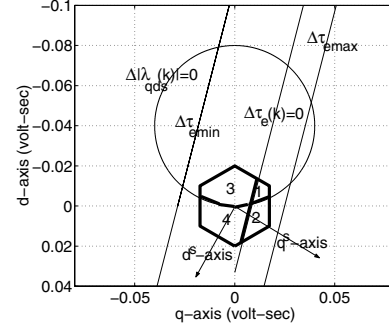


Fig. 6. Graphical representation of operating regions for steady state conditions

Any $\Delta\tau_e$ lines to the right of the $\Delta\tau_e(k)=0$ line represent an increase in torque. Any $\Delta\tau_e$ lines to the left of $\Delta\tau_e(k)=0$ represent a decrease in torque. Any $\Delta|\boldsymbol{\lambda}_{qds}(k)|$ circles within the $\Delta|\boldsymbol{\lambda}_{qds}(k)|=0$ circle represent a decrease in stator flux magnitude. Any $\Delta|\boldsymbol{\lambda}_{qds}(k)|$ circles outside $\Delta|\boldsymbol{\lambda}_{qds}(k)|=0$ represent an increase in flux. Thus it is seen that there are four operating regions within the hexagon as shown:

1. Increase torque, decrease flux
2. Increase torque, increase flux
3. Decrease torque, decrease flux
4. Decrease torque, increase flux

The standard table look up method of direct torque control allows only the voltage vectors represented by the vertices of the hexagon (plus the two zero vectors) to be selected for the duration of the sample period. However, if a pulse width modulation technique is used, an average voltage vector over the sample period can be synthesized which lies anywhere within the hexagon.

A control algorithm can be developed based on (8), (10) and Fig. 4 if $\Delta\tau_e(k)$ is set equal to $\tau_e(k)^* - \tau_e(k)$ and $\Delta|\boldsymbol{\lambda}_{qds}(k)| = |\boldsymbol{\lambda}_{qds}(k)|^* - \lambda_{ds}^e(k)$. The voltage vector calculated by the control algorithm is the intersection of the $\Delta\tau_e(k)^*$ line with the $\Delta|\boldsymbol{\lambda}_{qds}(k)|^*$ flux magnitude circle which is the solution of (8) and (10). The voltage vector can be synthesized using space vector modulation (SVM) techniques to calculate the inverter switch duty cycles [12]. Figure 7 shows the block diagram of the control system in which the proposed algorithm was implemented. (The additional voltage command, $V_{hfss}^*(k)$, is only necessary for the self-sensing position and speed estimation as explained in Section V.)

The control algorithm first tests if $\Delta\tau_e(k)^*$ is within the limits of $\Delta\tau_{emax}$ and $\Delta\tau_{emin}$. If it is not, $\Delta\tau_e(k)^*$ is set equal to the closest limit. There are then three possibilities for the voltage vector solution: the $\Delta\tau_e(k)^*$ line and the $\Delta|\boldsymbol{\lambda}_{qds}(k)|^*$ circle intersect within the allowable voltage hexagon, the $\Delta\tau_e(k)^*$ line and the $\Delta|\boldsymbol{\lambda}_{qds}(k)|^*$ circle intersect outside the allowable hexagon, or the $\Delta\tau_e(k)^*$ line and the $\Delta|\boldsymbol{\lambda}_{qds}(k)|^*$ circle do not intersect.

If the $\Delta\tau_e(k)^*$ line and the $\Delta|\lambda_{qds}(k)|^*$ circle intersect within the allowable voltage hexagon, the solution is the voltage vector defined by the intersection point closest to the origin and is implemented using space vector modulation.

If the $\Delta\tau_e(k)^*$ line and the $\Delta|\lambda_{qds}(k)|^*$ circle intersect outside of the allowable voltage hexagon, the desired voltage vector is again calculated; however, the magnitude is larger than what is available given the DC bus voltage. The magnitude of the voltage vector is reduced by the SVM algorithm until it lies on the hexagon boundary. This reduced magnitude voltage vector is then applied.

If the $\Delta\tau_e(k)^*$ line and the $\Delta|\lambda_{qds}(k)|^*$ circle do not intersect, this is an indication that a large change in torque is required. In this case, the maximum voltage vector in the direction of maximum change in torque is applied. This is the voltage vector perpendicular to the $\Delta\tau_e(k)^*$ line with the maximum magnitude allowed by the hexagon.
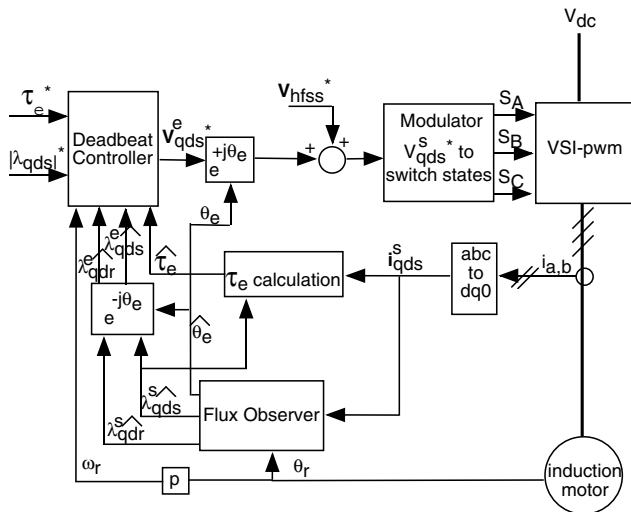


Fig. 7. Proposed deadbeat control block diagram

## III. SIMULATION RESULTS

The experimental motor used in this paper is a specially designed high speed (rated speed just over 23,000 rpm) induction machine for a NASA electro-mechanical actuator research project. The parameter values are given in the Appendix. The simulation conditions are set to match the experimental conditions. Experimentally, the machine was limited to 10,000 rpm or less due to concern about the condition of the bearings. All of the simulations neglect the PWM switching harmonics.

The controller was analyzed in two ways. First, to investigate its small signal stability, the operating point model was formed using the Matlab LTI function. To form the operating point model, the mechanical dynamics were neglected (constant speed) and perfect flux estimation was assumed (the flux observer was not included in the operating point model). Pole-zero migration plots were then created for a range of speeds from low speed to rated speed (180 rpm to 23,000 rpm) at the rated torque and rated flux operating point.

The second analysis was based on a time domain, nonlinear model simulation of the complete system including the flux observer and the mechanical dynamics. The speed, torque and stator flux responses to a square wave torque command are shown.

Figure 8 shows the pole-zero migration plot from the LTI analysis for a 100 μsec sample time (used experimentally). The result is seen to approximate the expected deadbeat response but there is not exact pole-zero cancellation and the free pole is not exactly at the origin. This improves as a smaller and smaller sample time is used. (The NASA motor has relatively small time constants as can be seen in the Appendix.)
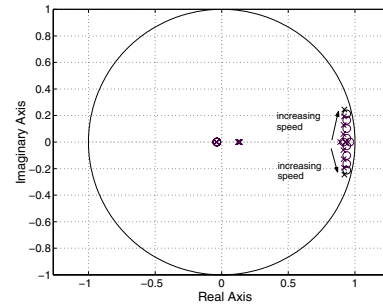


Fig. 8. Pole-Zero plot for 100 μsec sample time and no calculation delay

The time domain results shown in Figs. 9 and 10 demonstrate good performance. The torque response is seen to be a square wave as expected. Figure 10 also shows the effect of neglecting the resistance in deriving (9). For a stator resistance equal to zero, the stator flux is at the commanded value of 1 per unit. However, the stator flux magnitude is slightly reduced from the commanded value for a stator resistance of 0.18 ohms.
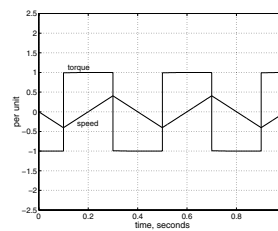


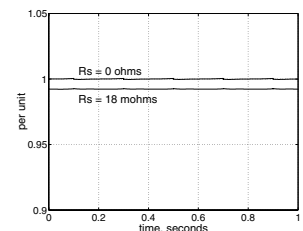Fig. 9. Torque and speed response for a 100 μsec sample time and no calculation delay

Fig. 10. Stator flux magnitude for 100 μsec sample time, no calculation delay and two values of stator resistance

In the ideal case, it is assumed that the command values for the manipulated variables ($V_{qs}^{s*}(k)$, $V_{ds}^{s*}(k)$) are calculated in zero time based on the present sampled value of the measured feedback variables ($i_{qs}(k)$, $i_{ds}(k)$). Realistically, however, there will be a calculation delay between when the feedback variables are measured and when the commanded values for the manipulated variables are updated because the required microprocessor calculations can not be done in zero time.

The command values for the manipulated variables $V_{qs}^{s*}(k)$ and $V_{ds}^{s*}(k)$ ultimately become pulse width commands for the gate drives in the inverter. In this implementation, the sampling time is synchronized with the PWM generation. Thus the PWM timers are updated at the same time as the feedback variables are measured. This results in a one step time delay for the control because the PWM timers are updated based on the calculations from the feedback data of the previous sample.

The effect of this one step time delay can be seen in the pole-zero plot of Fig. 11. The free pole and the pole-zero cancellation pair that were at or near the origin in Fig. 8 have now moved to the edge of the unit circle. The time domain simulations also show a more oscillatory response as seen in Figs. 12 and 13.
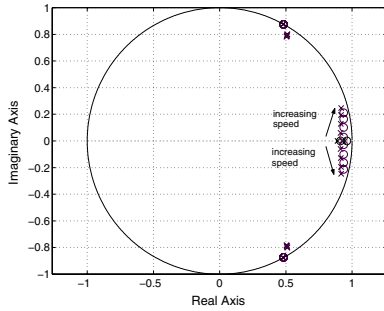


Fig. 11. Pole-Zero plot for 100 µsec sample time and one step time delay
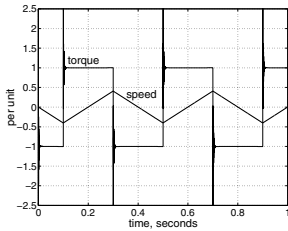


Fig. 12. Torque and speed response for a 100 µsec sample time and a 1 time step calculation delay
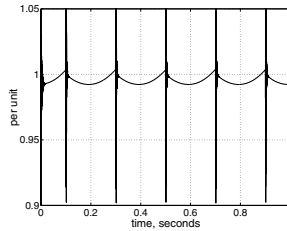
Figure 13. Stator flux magnitude for 100 µsec sample time and a 1 time step calculation delay

For a similar deadbeat type of controller, Ref [5] shows that a modification to $\Delta\tau_e(k)^*$ and $\Delta|\lambda_{qds}(k)|^*$ will move the system poles to lie further within the unit circle and reduce the oscillations. A similar derivation can be shown here. To include the one-step time delay, (7) can be expressed as shown in (19).

$$\frac{\tau_e(k+2)-\tau_e(k+1)}{t_s} = \tau_e(k+1)\left(\frac{-R_r}{\sigma L_r} - \frac{R_s}{\sigma L_s}\right) + \frac{3PL_m}{4\sigma L_s L_r}$$
$$\{-\omega_r\lambda_{ds}^e(k+1)\lambda_{dr}^e(k+1) + V_{qs}^e(k)^*\lambda_{dr}^e(k+1) - V_{ds}^e(k)^*\lambda_{qr}^e(k+1)\}$$
$$(19)$$

From (8) the expression for the control variables $V_{qs}^{e*}(k)$ and $V_{ds}^{e*}(k)$ is

$$V_{qs}^{e*}(k)t_s - V_{ds}^{e*}(k)t_s\frac{\lambda_{qr}^e(k)}{\lambda_{dr}^e(k)} = \omega_r\lambda_{ds}^e(k)\,t_s\,+$$

$$\frac{4\sigma L_s L_r}{3PL_m\lambda_{dr}^e(k)}\left(\tau_e(k)^* - \tau_e(k) + \tau_e(k)\left(\frac{R_r}{\sigma L_r} + \frac{R_s}{\sigma L_s}\right)t_s\right) \quad (20)$$

Under constant stator flux operation and assuming that $\lambda_{qdr}^e(k+1) \approx \lambda_{qdr}^e(k)$, (19) and (20) can be combined to form an approximate relationship between the commanded torque and the actual torque as shown in (21).

$$\tau_e(k+2) - \tau_e(k+1) = \tau_e(k+1)\left(\frac{-R_r}{\sigma L_r} - \frac{R_s}{\sigma L_s}\right)t_s + \tau_e(k)^*$$

$$- \tau_e(k) + \tau_e(k)\left(\frac{R_r}{\sigma L_r} + \frac{R_s}{\sigma L_s}\right)t_s \quad (21)$$

From (21), the characteristic equation of this simplified transfer function is

$$z^2 - z\left(1-\left(\frac{R_r}{\sigma L_r} + \frac{R_s}{\sigma L_s}\right)t_s\right) + \left(1-\left(\frac{R_r}{\sigma L_r} + \frac{R_s}{\sigma L_s}\right)t_s\right) = 0. \quad (22)$$

The magnitude of the poles of (22) is given in (23). For small values of $t_s$, these poles can be seen to lie close to the unit circle boundary. This indicates that the deadbeat controller is very sensitive to the one step time delay.

$$|p_1| = |p_2| = \sqrt{\left(1-\left(\frac{R_r}{\sigma L_r} + \frac{R_s}{\sigma L_s}\right)t_s\right)} \quad (23)$$

One way to reduce the sensitivity of the controller to the one step calculation delay is to relax the response required. Instead of a deadbeat response, an exponential response with a small time constant can be defined. The controller with the exponential response is much less sensitive to the one step calculation delay [13].

If the commanded change in torque, $\Delta\tau_e(k)^*$, in (8) and the commanded change in flux magnitude, $\Delta|\lambda_{qds}(k)|^*$, in (10) are reduced by a factor C, as shown in (24) and (25), the result is an exponential response. This can be seen by substituting the commanded values given in (26) into (7). The result is shown in (27).

$$\Delta\tau_e(k)^* = C\,(\tau_e(k)^* - \tau_e(k)) \quad (24)$$

$$\Delta|\lambda_{qds}(k)|^* = C\,(|\lambda_{qds}(k)|^* - |\lambda_{qds}(k)|) \quad (25)$$

$$V_{qs}^{e*}(k)t_s - V_{ds}^{e*}(k)t_s\frac{\lambda_{qr}^e(k)}{\lambda_{dr}^e(k)} = \omega_r\lambda_{ds}^e(k)\,t_s\,+$$

$$\frac{4\sigma L_s L_r}{3PL_m\lambda_{dr}^e(k)}\left(\tau_e(k)^* - \tau_e(k) + \tau_e(k)\left(\frac{R_r}{\sigma L_r} + \frac{R_s}{\sigma L_s}\right)t_s\right) \quad (26)$$

$$\tau_e(k+1) = C\tau_e(k)^* + \tau_e(k)(1-C) \qquad (27)$$

Taking the z-transform of (27) results in the expected transfer function for an exponential response [14].

$$\frac{\tau_e(z)}{\tau_e(z)^*} = \frac{C}{z-(1-C)} \qquad (28)$$

To see the effect of the one-step calculation delay, (26) is substituted into (18) instead of (7). The result is given in (29) with the same assumptions given previously—that is, $\lambda_{qdr}^e(k+1) \approx \lambda_{qds}^e(k)$ and $\lambda_{qdr}^e(k+1) \approx \lambda_{qdr}^e(k)$.

$$\tau_e(k+2) - \tau_e(k+1) = \tau_e(k+1)\left(\frac{-R_r}{\sigma L_r} - \frac{R_s}{\sigma L_s}\right)t_s + C\tau_e(k)^*$$

$$- C\tau_e(k) + \tau_e(k)\left(\frac{R_r}{\sigma L_r} + \frac{R_s}{\sigma L_s}\right)t_s \qquad (29)$$

The z-transform of (29) results in the transfer function shown in (30).

$$\frac{\tau_e(z)}{\tau_e(z)^*} = \frac{C}{z^2 - z\left(1-\left(\frac{R_r}{\sigma L_r} + \frac{R_s}{\sigma L_s}\right)t_s\right) + \left(C-\left(\frac{R_r}{\sigma L_r} + \frac{R_s}{\sigma L_s}\right)t_s\right)} \qquad (30)$$

The magnitude of the poles of the transfer function in (30) is shown in (31). It can be seen that for C<1 the poles will move further inside the unit circle and the response is expected to be less oscillatory.

$$|p_1| = |p_2| = \sqrt{\left(C-\left(\frac{R_r}{\sigma L_r} + \frac{R_s}{\sigma L_s}\right)t_s\right)} \qquad (31)$$

The simulation results show this to be the case. Figure 14 shows the LTI pole-zero migration plot for the controller with the commanded torque and stator flux magnitude values given by (24) and (25) respectively and C=0.8. The poles have clearly moved further inside the unit circle. The time domain simulation results given in Figs. 15 and 16 show reduced overshoot and oscillation in the response.
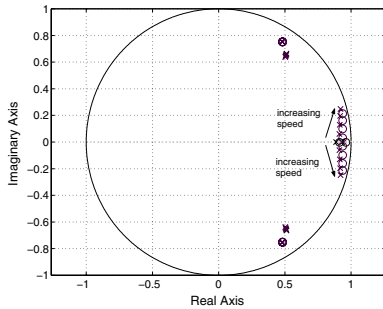


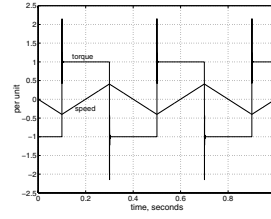Fig. 14. Pole-Zero plot for 100 μsec sample time, one step time delay and C=0.8



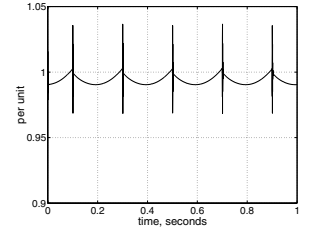Fig. 15. Torque and speed response for a 100 μsec sample time,1 time step delay and C=0.8



Fig. 16. Stator flux magnitude for a 100 μsec sample time,1 time step delay and C=0.8

## IV. EXPERIMENTAL RESULTS

The experimental test set up consisted of a dc power supply, an intelligent power module, a dSpace 1103[1] digital controller and the NASA test motor. The results were captured using dSpace software. The data files were then plotted using Matlab. Two phase currents were measured and an encoder was used for position feedback. The position feedback was necessary because a flux observer based on the current model was used. (In Section V, the position feedback is provided by the self-sensing algorithm and the encoder information was used for comparison purposes only.) The speed was calculated in the controller using the position information. The torque and flux were estimated in the controller using current and position information.

Figures 17 and 18 show the torque, stator flux and speed for the same conditions as in Figs. 15 and 16 in simulation.
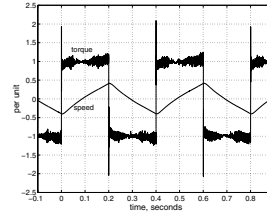


Fig. 17. Experimental results: torque and speed response for a 100 μsec sample time, one time step delay and C=0.8

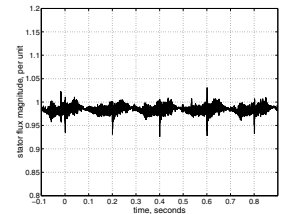

Fig. 18. Experimental results: stator flux magnitude for a 100 μsec sample time, one time step delay and C=0.8

In general, the response is as predicted. In the actual implementation, there is always a deadtime, or blanking time, in the inverter so that the two switches across a leg do not conduct at the same time. In addition, there is a voltage drop across the conducting devices. Both of these effects result in a lower voltage being applied to the machine than is actually commanded. This "deadtime voltage" can be calculated [15].

$$V_{deadtime} = \frac{4V_d}{3} \; e^{j(k-1)\frac{\pi}{3}} \qquad (32)$$

$V_d$ is the magnitude of the voltage due to the combination of the deadtime losses and the conduction losses and k is the sector of the d-q plane in which the current vector is located, k=1,2...6. This controller was found to be sensitive to deadtime compensation as can be seen by comparing Figs. 19 and 20 (without deadtime) to Figs. 17 and 18 (with deadtime). It is seen that without deadtime compensation, both the torque and stator flux magnitudes were reduced.
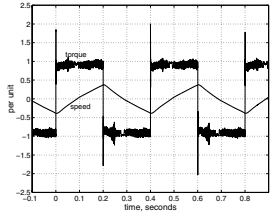



Fig. 19. Experimental results: torque and speed response for a 100 μsec sample time, one time step delay and C=0.8, no deadtime compensation
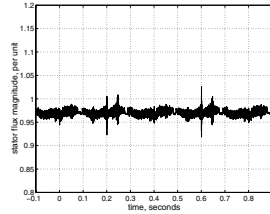
Fig. 20. Experimental results: stator flux magnitude for a 100 μsec sample time, one time step delay and C=0.8, no deadtime compensation

## V. LOW SPEED SENSORLESS IMPLEMENTATION

To date, the self-sensing method has been demonstrated only with the field orientation method of control. The use of self-sensing in a deadbeat direct torque control offers the potential of full speed range sensorless operation with the flux estimate based on the back emf method at higher speeds and on the self-sensing position estimate at lower speeds.

To estimate the rotor position angle, $\theta_r$, the self-sensing technique requires a machine with a magnetic saliency related to the rotor position [10]. The NASA motor rotor was designed to produce a position dependent magnetic saliency by changing the shape of the rotor bars as a function of position as shown in Fig. 21. (The rotor is 1.3 inches in diameter).
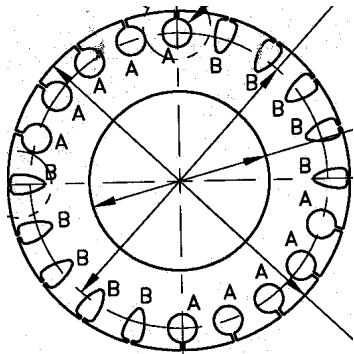


Fig. 21. Rotor cross-section of NASA machine

Additionally, the self-sensing technique requires a high frequency carrier signal. The structure of a deadbeat type of direct torque control lends itself to the use of the self-sensing method of position estimation because the necessary high frequency signal can be easily added to the fundamental voltage command as shown in Fig. 7. Thus the commanded voltage into the pwm modulator will consist of the fundamental voltage command, $V_{qds}^{s*}(k)$ and the high frequency voltage, $V_{hfss}^{*}(k)$. The resulting current is filtered as described in [14] and a signal at twice the rotor position is generated due to the position dependent magnetic saliency. This signal can be tracked in a closed loop, saliency image-tracking observer to produce position, velocity, acceleration, and disturbance torque estimates.

Figures 22 and 23 show the results of a no load closed loop low speed sensorless control using the self-sensing position estimate as feedback for the controller. Figure 22 shows the spectra of the negative sequence current (as defined in [16]) for a constant 3 Hz speed. The component due to the rotor saliency is clearly visible at 6 Hz. Figure 23 shows a no load speed reversal from –3 Hz to + 3 Hz.
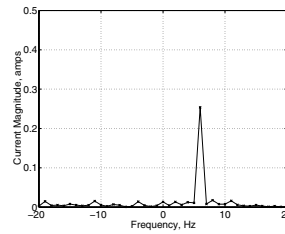



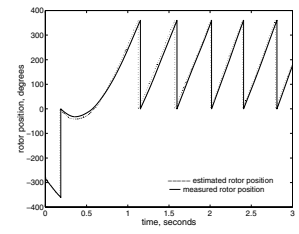Fig. 22. Negative sequence current spectra for constant speed 3 Hz operation

Fig. 23. Sensorless speed reversal of proposed controller with estimated rotor position and speed feedback based on self-sensing method

## VI. CONCLUSIONS

This paper has developed a new, deadbeat direct torque control method based on stator and rotor flux as state variables. This choice of state variables allows a clear graphical visualization of the voltage vector solution and the inverter operating limits.

The implementation of the proposed controller was evaluated experimentally and found to produce good results. The implementation issues which could limit performance were also evaluated.

The controller was found to be sensitive to the one step time delay in the experimental implementation. The deadtime voltage drop, without appropriate compensation, was also found to reduce the torque and flux in the machine.

The structure of the proposed controller allows the addition of a high frequency voltage vector to the commanded fundamental voltage vector. This allows the self-sensing method of position and speed estimation to be used thus demonstrating low, including zero speed, sensorless control.

## APPENDIX

NASA Motor: 2 pole induction, 96 $V_{LN}$, 400 Hz, $L_m$=1.9e-3 H., $L_{ls}$=1.25e-4 H., $L_{lr}$=1.25e-4 H., $R_r$=.105 Ω., $R_s$=.09 Ω., J=1.02e-4 kg-m$^2$, $\tau_{em}$=1 N-m, $\omega_r$=23,030 rpm

REFERENCES

[1] Takahashi, Isao and Noguchi, Toshihiko; "A New Quick-Response and High-Efficiency Control Strategy of an Induction Motor," *IEEE Transactions on Industry Applications*, Vol. IA–22, No. 5, Sept./Oct. 1986, pp. 820–827.

[2] Depenbrock, M., "Direct Self-Control (DSC) of Inverter-Fed Induction Machine," *IEEE Transactions on Power Electronics*, Vol. 3, No. 4, October, 1988, pp. 420–429.

[3] Pekka Tiitinen, "The Next Generation Motor Control Method, DTC, Direct Torque Control," *Proc. 1996 International Conf. on Power Electronics, Drives and Systems for Industrial Growth*, New Delhi, India, Jan. 8–11, 1996, pp. 37–43.

[4] Habetler, Thomas, Profumo, Francesco, Pastorelli, Michele, Tolbert, Leon, "Direct Torque Control of Induction Machines Using Space Vector Modulation," *IEEE Trans on Industry Applications*, Vol. 28, No. 5, Sept./Oct. 1992, pp. 1045–1053.

[5] Maes, Jehudi, Jan Melkebeek, "Discrete Time Direct Torque Control of Induction Motors using Back-EMF Measurement," *Proc. of IEEE Industrial Applications Society Conf.,* St. Louis, Mo., Oct. 12–15, 1998, pp. 407–414.

[6] Neves, Francisco, Benjamim Menezes, Selenio Silva, "A Deadbeat Torque and Flux Field Oriented Controller for Induction Motor Drives,*" Proc. of XII Brazilian Automatic Control Conference*, Vol. VI, Sept. 1998, pp. 2243–2247.

[7] Buja, G., M. Candela, R. Menis, "A Novel Direct Control Scheme for SVM Inverter-Fed Induction Motor Drives," *Proceedings of 1999 ISIE*, Bled, Slovenia, pp. 1267–1272.

[8] Casadei, Domenico, Giovanni Serra, Angelo, Tani, "Analytical Investigation of Torque and Flux Ripple in DTC Schemes for Induction Motors," *IECON Proceedings of the 1997 23$^{rd}$ Annual International Conference on Industrial Electronics, Control, and Instrumentation*, New Orleans, Louisiana, Nov. 9–14, 1997, Vol. 2, pp. 552–556.

[9] Casadei, Domenico, Giovanni Serra, Angelo, Tani, "Implementation of a Direct Torque Control algorithm for Induction Motors Based on a Discrete Space Vector Modulation," *Proceedings of the 1998 IEEE Power Electronics Specialists Conference*, Fukuoka, Japan, May 18–21, 1998, Vol. 2, pp. 997–1003.

[10] Jansen, Patrick L. and Robert D. Lorenz, "Transducerless Position and Velocity Estimation in Induction and Salient AC Machines," *IEEE Trans. on Industry Applications*, Vol. 31, No. 2, March/April 1995, pp. 240–247.

[11] Novotny, Donald W. and Thomas A. Lipo; *Vector Control and Dynamics of AC Drives*, Oxford University Press, New York, 1996.

[12] van der Broeck, H.W., Skudelny, H.C. and Stanke, G. "Analysis and Realization of a Pulse Width Modulator Based on Voltage Space Vectors," *IEEE Transactions on Industry Applications*, Vol. 24, No. 1, Jan./Feb. 1988, pp. 142–150.

[13] Kenny, B.H., *Deadbeat Direct Torque Control of Induction Machines Using Self-Sensing at Low and Zero Speeds*, Ph.D. thesis, UW-Madison, 2001.

[14] Bollinger, J.G. and Duffie, N.A., *Computer Control of Machines and Processes*, Addison-Wesley Publishing Company, New York, 1988.

[15] Vas, Peter *Sensorless Vector and Direct Torque Control*, Oxford, U.K.; Oxford University Press, 1998.

[16] Degner, Michael and Lorenz, Robert, "Using Multiple Saliencies for the Estimation of Flux, Position, and Velocity in AC Machines," *IEEE Transactions on Industrial Applications,* Vol. 34, No. 5, Sept./Oct. 1998, pp. 1097–1104.

# REPORT DOCUMENTATION PAGE

Public reporting burden for this collection of information is estimated to average 1 hour per response, including the time for reviewing instructions, searching existing data sources, gathering and maintaining the data needed, and completing and reviewing the collection of information. Send comments regarding this burden estimate or any other aspect of this collection of information, including suggestions for reducing this burden, to Washington Headquarters Services, Directorate for Information Operations and Reports, 1215 Jefferson Davis Highway, Suite 1204, Arlington, VA 22202-4302, and to the Office of Management and Budget, Paperwork Reduction Project (0704-0188), Washington, DC 20503.

| 1. AGENCY USE ONLY (*Leave blank*) | 2. REPORT DATE | 3. REPORT TYPE AND DATES COVERED |
|---|---|---|
| | September 2002 | Technical Memorandum |

**4. TITLE AND SUBTITLE**

Stator and Rotor Flux Based Deadbeat Direct
Torque Control of Induction Machines

**5. FUNDING NUMBERS**

WU–755–1A–11–00

**6. AUTHOR(S)**

Barbara H. Kenny and Robert D. Lorenz

**7. PERFORMING ORGANIZATION NAME(S) AND ADDRESS(ES)**

National Aeronautics and Space Administration
John H. Glenn Research Center at Lewis Field
Cleveland, Ohio 44135–3191

**8. PERFORMING ORGANIZATION REPORT NUMBER**

E–12945–1

**9. SPONSORING/MONITORING AGENCY NAME(S) AND ADDRESS(ES)**

National Aeronautics and Space Administration
Washington, DC 20546–0001

**10. SPONSORING/MONITORING AGENCY REPORT NUMBER**

NASA TM—2001-211100-REV1

**11. SUPPLEMENTARY NOTES**

Prepared for the 2001 Industry Applications Society Annual Meeting sponsored by the Institute of Electrical and Electronics Engineers, Chicago, Illinois, September 30–October 5, 2001. Barbara H. Kenny, NASA Glenn Research Center; Robert D. Lorenz, University of Wisconsin, Madison, Department of ECE and ME, 1513 University Avenue, Madison, Wisconsin 53706. Responsible person, Barbara H. Kenny, organization code 5450, 216–433–6289.

**12a. DISTRIBUTION/AVAILABILITY STATEMENT**

Unclassified - Unlimited
Subject Category: 33          Distribution: Nonstandard

Available electronically at http://gltrs.grc.nasa.gov

This publication is available from the NASA Center for AeroSpace Information, 301–621–0390.

**12b. DISTRIBUTION CODE**

**13. ABSTRACT** *(Maximum 200 words)*

A new, deadbeat type of direct torque control is proposed, analyzed, and experimentally verified in this paper. The control is based on stator and rotor flux as state variables. This choice of state variables allows a graphical representation which is transparent and insightful. The graphical solution shows the effects of realistic considerations such as voltage and current limits. A position and speed sensorless implementation of the control, based on the self-sensing signal injection technique, is also demonstrated experimentally for low speed operation. The paper first develops the new, deadbeat DTC methodology and graphical representation of the new algorithm. It then evaluates feasibility via simulation and experimentally demonstrates performance of the new method with a laboratory prototype including the sensorless methods.

**14. SUBJECT TERMS**

Direct torque control; Sensorless control; Induction machine; Deadbeat control

**15. NUMBER OF PAGES**
15

**16. PRICE CODE**

| 17. SECURITY CLASSIFICATION OF REPORT | 18. SECURITY CLASSIFICATION OF THIS PAGE | 19. SECURITY CLASSIFICATION OF ABSTRACT | 20. LIMITATION OF ABSTRACT |
|---|---|---|---|
| Unclassified | Unclassified | Unclassified | |

NSN 7540-01-280-5500

Standard Form 298 (Rev. 2-89)
Prescribed by ANSI Std. Z39-18
298-102